Optimal control over high-order-harmonic ellipticity in two-color cross-linearly-polarized laser fields

Yiqi Fang[1] and Yunquan Liu[1,2,3,4,*]

[1]*State Key Laboratory for Mesoscopic Physics and Frontiers Science Center for Nano-Optoelectronics, School of Physics, Peking University, Beijing 100871, China*

[2]*Collaborative Innovation Center of Quantum Matter, Beijing 100871, China*

[3]*Collaborative Innovation Center of Extreme Optics, Shanxi University, Taiyuan, Shanxi 030006, China*

[4]*Center for Applied Physics and Technology, HEDPS, Peking University, Beijing 100871, China*

(Received 28 September 2020; accepted 10 March 2021; published 24 March 2021)

We investigate the generation of high-order harmonics with arbitrary ellipticity using synthesized two-color (800-nm + 400-nm) cross-linearly-polarized laser fields. It is shown that one can realize control over harmonic ellipticity by finely adjusting the relative phase and the crossing angle of such two-color fields. Through analyzing the time-frequency distributions and the quantum orbits of harmonic radiations, we show that the harmonic helicity is originated from the unsymmetrical contribution between different quantum orbits released in one 800-nm cycle. And, we further reveal that the controllability of harmonic ellipticity in such two-color fields is closely related to the modulation of crossing angle and relative phase on the driving light's spin angular momentum. Finally, we show the probability of producing and modulating isolated helical attosecond pulses with few-cycle two-color cross-linearly-polarized laser fields.

DOI: 10.1103/PhysRevA.103.033116

I. INTRODUCTION

The development of light sources with attosecond timescales facilitates the capture and control of ultrafast physical processes [1]. The high-order harmonic generation (HHG) in the intense laser atom interaction enables the coherently upconverting of the fundamental laser pulses, to produce the attosecond burst of extreme ultraviolet (EUV) radiation [2,3]. HHG process is typically described in terms of the semiclassical three-step model [4]. Because of the growing interest in probing EUV and x-ray circular dichroism and photoelectron chirality in matter, HHG with controllable ellipticity has become of great interest [5]. The polarization state of high-harmonic beams is closely related to the ellipticity of the driving laser [6]. However, when increasing the ellipticity, the recollision probability of electrons will quickly decrease, which consequently leads to the dramatically decreasing harmonic generation efficiency [7,8].

There have been several methods proposed to circumvent this difficulty [9–12]. Employing collinear two-color counter-rotating circularly polarized laser fields, one can access the bright EUV radiation consisting of pairs of highly helical harmonics with orders $3n+1$ and $3n-1$ [13,14]. However, as the pairs of adjacent order harmonics appear of opposite helicity, the synthesized attosecond pulses would manifest nearly linear polarization. To overcome this flaw, an improved noncollinear circularly polarized scheme was proposed, which can produce isolated circularly polarized high-harmonic pulses [15–17]. Recently, a time-domain approach using the superposition of two independent orthogonally polarized EUV sources was presented [18]. This scheme can realize the direct ellipticity control in analogy with visible light. Due to the intrinsic angular momentum conservation and parity conservation, these methods are fundamentally unable to generate the bright high-order harmonics covering all integer orders.

On the other hand, the two-color cross-linearly-polarized laser fields with typically parallel and orthogonal polarizations have also been widely applied in HHG [19–24], which can also be used to generate elliptical high-order harmonics [25–28]. In the geometry of two-color cross-linearly-polarized laser fields, the crossing angle and the relative phase are two important parameters. HHG using such laser fields at specific crossing angles has been studied [25–27]. And the influence of the relative phase, which would provide alternative freedom to control the harmonic ellipticity, has never been revealed, to the best of our knowledge. To realize the optimal control over harmonic ellipticity in two-color cross-linearly-polarized fields, the comprehensive control of harmonic ellipticity by jointly adjusting these two parameters is requisite.

In this paper, we theoretically study the modulation of high-order-harmonic ellipticity by using two-color cross-linearly-polarized laser fields. Within the framework of the strong-field approximation (SFA) [29], we show the dependence of harmonic ellipticity on the crossing angle and the relative phase of such two-color fields. In particular, two features of the ellipticity modulation are revealed: (i) when increasing the crossing angle, the harmonic ellipticity is not monotonously increased; (ii) the crossing angle and the relative phase have different effects on controlling the harmonic ellipticity. Based on the time-frequency analysis

*yunquan.liu@pku.edu.cn

[30] and the quantum-orbit analysis [31], we show that the asymmetry between different quantum orbits' recollision dynamics, i.e., their positions and velocities at the moment of recollision, determines the high-order-harmonic helicity, leading to feature (i). As for (ii), we inspect the instantaneous spin angular momentum (SAM) of the driving light fields. We find that the difference between the crossing angle and the relative phase in ellipticity control is attributed to their different effects on the driving field's SAM. The paper is organized as follows. In Sec. II, we present the theoretical model and the simulation results. We interpret our calculations in Sec. III, in which we investigate the harmonics' temporal distributions, recollision electron trajectories and the time-dependent SAM structures of the driving laser fields, respectively. In Sec. IV, we present the simulation of isolated attosecond pulse produced by the few-cycle driving fields. Finally, we conclude our study in Sec. V.

II. THEORETICAL MODEL AND RESULTS

A. Theoretical model

According to the SFA, the time-dependent dipole moment $\mathbf{D}(t)$ can be written as

$$\mathbf{D}(t) = -i\int_{-\infty}^{t} dt' \left[\frac{-2\pi i}{t-t'-i\delta}\right]^{3/2} \mathbf{d}^*[\mathbf{p}_s(t',t)+\mathbf{A}(t)]\mathbf{E}(t') \times \mathbf{d}[\mathbf{p}_s(t',t)+\mathbf{A}(t')]e^{-iS(t',t)} + \text{c.c.}, \quad (1)$$

in which $\mathbf{E}(t)$ is the electric field, $\mathbf{A}(t) = -\int_{-\infty}^{t} dt'\mathbf{E}(t')$ is the vector potential of the laser field, δ is an arbitrary small positive regularization constant introduced to smooth out the singularity, $\mathbf{d}[\mathbf{p}_s(t',t)+\mathbf{A}(t')]$ is the dipole transition matrix element from ground state to plane wave state, and $\mathbf{d}^*[\mathbf{p}_s(t',t)+\mathbf{A}(t)]$ is the dipole transition matrix element for the recombination process. Here, the ground state of the hydrogenlike atoms is assumed in calculating the transition dipoles. Specifically, the dipole transition maxtrix elements $\mathbf{d}(\mathbf{p})$ are given by $\mathbf{d}(\mathbf{p}) = i(\frac{2^{7/2}\alpha^{5/4}}{\pi})\frac{\mathbf{p}}{(p^2+\alpha)^3}$, in which $\alpha = 2I_p$ and I_p is ionization potential of the target atoms. Also, $\mathbf{p}_s = -\frac{1}{t-t'}\int_{t'}^{t}\mathbf{A}(t'')dt''$ is the saddle point momentum which is calculated from the saddle point equation $\nabla_{\mathbf{p}}S(t,t') = 0$. Here $S(t,t') = \int_{t'}^{t} dt''(\frac{1}{2}[\mathbf{p}+\mathbf{A}(t'')]^2 + I_p)$ is referred to as the quasiclassical action. The saddle-point approximation for the integral over $\mathbf{p}$ yields a factor $(t-t')^{-3/2}$ that accounts for the quantum diffusion effect. Accordingly, the electric field of high-order harmonic can be calculated from the Fourier components of $\mathbf{D}(t)$ as

$$\mathbf{E}_q \propto \omega_q^2 \int \mathbf{D}(t)e^{-i\omega_q t}dt, \quad (2)$$

where $\omega_q = q\omega_{800}$ is the frequency of the qth harmonic and ω_{800} is the 800-nm light frequency. Then, the qth harmonic's ellipticity can be expressed by [27]

$$\varepsilon_q = \tan\{\text{asin}[\sin[2\text{atan}(|E_{q,x}|/|E_{q,y}|)]\sin(\phi_{q,x}-\phi_{q,y})]/2\}. \quad (3)$$

Here, $E_{q,x}$ and $E_{q,y}$ are the x- and y-component electric fields, whose phases are given by $\phi_{q,x} = \text{atan}[\text{Im}(E_{q,x})/\text{Re}(E_{q,x})]$ and $\phi_{q,y} = \text{atan}[\text{Im}(E_{q,y})/\text{Re}(E_{q,y})]$, respectively.

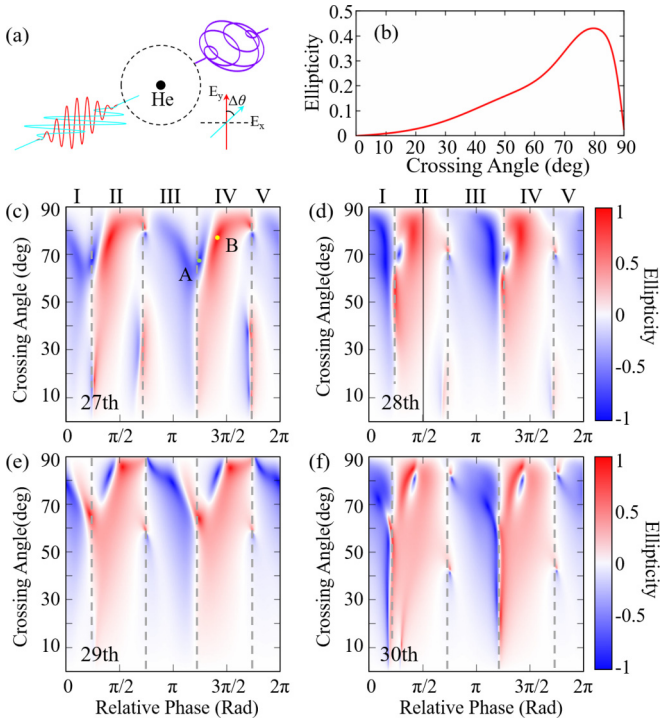

FIG. 1. (a) Illustration of producing the elliptical high-order harmonics in the two-color cross-linearly-polarized laser field. (b) The ellipticity (ε) distribution of the 28th harmonic with respect to the crossing angle. The relative phase is $\pi/2$, i.e., the black solid line in (d). (c)–(f) The ellipticity distributions (color scale) of the 27th-30th harmonics as a function of the relative phase and crossing angle. For each harmonic, to facilitate the observation, the distributions are separated into five regions (I, II, III, IV, and V). In (c), the A point ($\Delta\theta = 67.4^\circ$, $\Delta\varphi = 3.9$ rad, $\varepsilon_q = -0.93$) and B point ($\Delta\theta = 76.8^\circ$, $\Delta\varphi = 4.5$ rad, $\varepsilon_q = 0.98$) indicate the conditions, in which the harmonics are nearly circularly polarized.

B. Ellipticity features of harmonics in two-color cross-linearly-polarized fields

Without losing generality, we use the model He atom as the target, which can exclude the effect of nonzero orbital angular momentum state of bound atomic electrons [32]. The intensities of 800-nm and 400-nm light field are chosen to be $I_{800} = I_{400} = 7\times10^{13}$ W/cm^2. As shown in Fig. 1(a), the polarization of 800-nm light is aligned along the y direction. For simulations, the synthesized two-color electric field is given by

$$\mathbf{E}(t) = [E_{800}f(t)\cos(\omega_{800}t) + E_{400}f(t)\cos(\Delta\theta)\cos(\omega_{400}t-\Delta\varphi)]\mathbf{e}_y + E_{400}f(t)\sin(\Delta\theta)\cos(\omega_{400}t-\Delta\varphi)\mathbf{e}_x, \quad (4)$$

where E_{800} and E_{400} are the peak electric field strength of 800- and 400-nm field, respectively. $\Delta\theta$ is the crossing angle between these two light field polarizations, $\Delta\varphi$ is their relative phase, and $f(t)$ is the pulse envelope (a ten-cycle trapezoidal envelope is used).

Here, we simulate the harmonic fields near the cut-off region of HHG spectra, in which SFA could have a more accurate resemblance with the results from time-dependent

Schrödinger equation [33]. In Figs. 1(c)–1(f), we present the ellipticity distributions as a function of the crossing angle and the relative phase. Closer inspection indicates that highly helical harmonics can be obtained at suitable parameters. For example, the ellipticity of the 27th harmonic reaches $\varepsilon_{27} = -0.93$ at $\Delta\theta = 67.4^\circ$ and $\Delta\varphi = 3.9$ rad [A point in Fig. 1(c)]. A reversed high ellipticity $\varepsilon_{27} = 0.98$ can be reached at $\Delta\theta = 76.8^\circ$ and $\Delta\varphi = 4.5$rad [B point in Fig. 1(c)]. Remarkably, such ellipticities are much higher than what can be obtained by directly using orthogonally polarized two-color laser fields [25].

One can notice that the harmonic ellipticity is not monotonously related to the crossing angle, as shown in Fig. 1(b). When increasing the crossing angle, the ellipticity slowly increases at first, and it will reach its maximum when the crossing angle is $\Delta\theta \sim 80^\circ$, then it will drop rapidly. At $\Delta\theta \sim 90^\circ$, the harmonic ellipticity unexpectedly becomes very small.

Also, it can be further noticed that there are some differences between the relative phase and the crossing angle in modulating the harmonic ellipticity. For the relative phase, it can significantly affect harmonic ellipticity's magnitude and sign. To facilitate the observation, we divide the ellipticity distribution of each harmonic into five phase regions [as shown in Figs. 1(c)–1(f)]. In the second and fourth regions (II and IV), the harmonic ellipticity is positive. In other regions (I, III, and V), the negative ellipticities are in the majority. Compared to the relative phase, the crossing angle has less influence on the sign of harmonic ellipticities. That is, for most relative phases, the sign of ellipticity is nearly unchanged when only varying the crossing angle. For example, if the relative phase is $\Delta\varphi = \pi/2$, the ellipticity of the 28th harmonic is always positive even when varying the crossing angle [see Fig. 1(b)]. The crossing angle mainly affects the magnitude of harmonic ellipticity.

III. ANALYSIS AND DISCUSSION

A. Gabor time-frequency analysis

First, we investigate the modulation of the crossing angle on harmonic ellipticity. To this end, the Gabor time-frequency analysis [30] is employed to access the temporal profiles of the harmonic radiations. The time-resolved harmonic electric field can be given by $\mathbf{E}'_q(t) \propto \omega_q^2 G_{\mathbf{D}}(t, \omega_q) = \omega_q^2 \int \mathbf{D}(\tau) g(\tau - t) e^{-i\omega_q \tau} d\tau$, where the Gaussian function $g(\tau - t)$ is chosen to be the window function. And the full width at half maximum (FWHM) of this Gaussian function is $T_{800}/40$ (T_{800} is one cycle of the 800-nm light field). Based on $\mathbf{E}'_q(t)$, the time-resolved ellipticity $\varepsilon'_q(t)$ can be obtained via Eq. (3). Importantly, the harmonic electric field $\mathbf{E}_q$ which was given by Eq. (2) can be recovered through integrating $\mathbf{E}'_q(t)$:

$$\int_{-\infty}^{\infty} \mathbf{E}'_q(t) dt = \omega_q^2 \int_{-\infty}^{\infty} \mathbf{D}(\tau) \left[\int_{-\infty}^{\infty} g(\tau - t) dt \right] e^{-i\omega_q \tau} d\tau = \mathbf{E}_q. \quad (5)$$

Equation (5) indicates that the harmonic field $\mathbf{E}_q$ can be regarded as the time accumulation of $\mathbf{E}'_q(t)$.

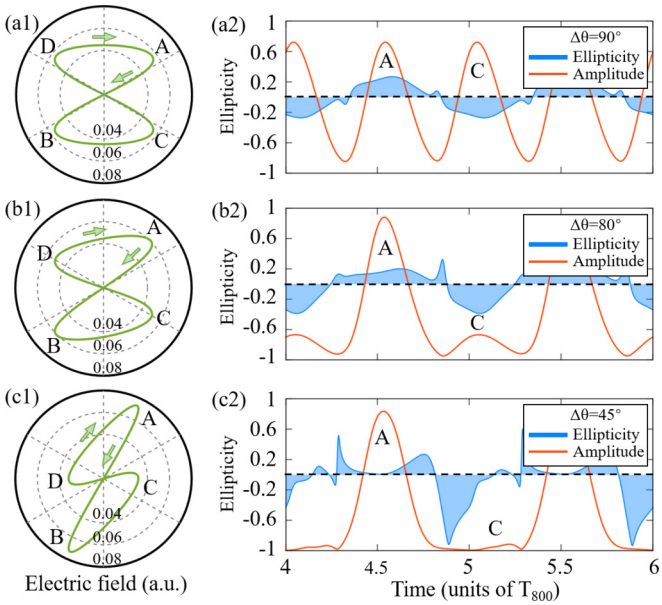

FIG. 2. Interpretation for the modulation of the harmonic ellipticity in the two-color cross-linearly-polarized field. First column: Lissajous curves (green) of the electric field of the driving two-color light field in one 800-nm light cycle (T_{800}). Second column: temporal distribution of 28th harmonic's ellipticity (blue) and amplitude (red), which is obtained by performing the Gabor transform. The distribution of amplitude is zoomed to be observable. The relative phase is $\Delta\varphi = \pi/2$ and the crossing angles are (a) $\Delta\theta = 90^\circ$, (b) $\Delta\theta = 80^\circ$, and (c) $\Delta\theta = 45^\circ$, respectively.

In Fig. 2, we present the Lissajous curves of the driving electric fields at different crossing angles (first column) and their 28th harmonics' temporal profiles (second column), i.e., $\mathbf{E}'_q(t)$ and $\varepsilon'_q(t)$. As shown, for two-color cross-linearly-polarized laser fields, there are four electric field peaks in one 800-nm light cycle (labeled by A, B, C, and D). The electrons released from the field peaks A and C are more likely to recollide with the nucleus [34]. As for the electrons born at the field peaks B and D, their recombination probabilities are much smaller [34]. Thus, there are two dominated harmonic bursts emitted in one 800-nm light cycle, corresponding to the field peaks A and C [35], as shown in Figs. 2(a2)–2(c2).

When the crossing angle is $\Delta\theta = 90^\circ$, the driving electric field peaks A and C have the same strength [Fig. 2(a1)]. Notably, their corresponding harmonic bursts A and C have the same amplitudes but reversed helicities [Fig. 2(a2)]. According to Eq. (5), after the accumulation of these two symmetrical harmonic bursts, the overall helicity of the 28th harmonic radiation $\mathbf{E}_{28}$ will cancel. Therefore, the ellipticity is small at $\Delta\theta = 90^\circ$ [see Fig. 1(b)]. When the crossing angle is $\Delta\theta = 80^\circ$, the harmonic burst C is suppressed [Fig. 2(b2)] as the corresponding electric field peak becomes weaker [Fig. 2(b1)]. The ellipticity distributions of the harmonic bursts A and C are not exactly opposite anymore. Because of such broken symmetry between these harmonic bursts, the 28th harmonic is elliptically polarized to some extent at $\Delta\theta = 80^\circ$ [see Fig. 1(b)]. With the crossing angle further reducing to $\Delta\theta = 45^\circ$, the dominated harmonic burst A does not have a significant ellipticity [Fig. 2(c2)]. In contrast, the

ellipticity of harmonic burst C is large, however, its amplitude is very small. Thus, in the case of $\Delta\theta = 45^\circ$, the overall harmonic ellipticity is much smaller than that at $\Delta\theta = 80^\circ$ [see Fig. 1(b)].

B. Quantum-orbit analysis

To further reveal the deeper mechanism of producing elliptical harmonics in two-color cross-linearly-polarized laser fields, we then perform the quantum-orbit analysis [31] for the inherent dependence of harmonic ellipticity on electron quantum orbits. The quantum orbits are the trajectories along which the phase of the multidimensional integral Eq. (1) is stationary. They can be numerically obtained by solving the saddle point equations:

$$\mathbf{p}_s = -\frac{1}{t_r - t_i}\int_{t_i}^{t_r} \mathbf{A}(t'')dt'', \tag{6}$$

$$[\mathbf{p}_s + \mathbf{A}(t_i)]^2 + 2I_p = 0, \tag{7}$$

$$[\mathbf{p}_s + \mathbf{A}(t_r)]^2 + 2I_p = 2\omega. \tag{8}$$

Here, $\mathbf{p}_s$ is the canonical momentum of the electrons, t_i is related to the moment of ionization, and t_r is associated with the recombination time. Equation (6) describes the return condition for the electrons. Equations (7) and (8) express energy conservation at the moment of ionization and recombination, respectively. Due to the constraint imposed by Eq. (7), all the solutions $\mathbf{p}_s$, t_i, and t_r are complex valued. To gain an intuitive picture about the quantum orbits, we inspect the real part of electron trajectories during the classical motion. For real times $t \in [\mathrm{Re}t_i, \mathrm{Re}t_r]$, the electron position $\mathbf{R}(t)$ is obtained by [36]

$$\mathbf{R}(t) = \mathrm{Re}\left[\mathbf{p}_s(t - t_i) + \int_{t_i}^{t} A(t')dt'\right]. \tag{9}$$

We solve Eqs. (6)–(8) for the 28th harmonic and plug the solutions into Eq. (9). The obtained electron trajectories are displayed in Figs. 3(a)–3(c). For each crossing angle, four electron trajectories (also labeled by A, B, C, and D) which correspond to the four electric field peaks, are presented. The directions of the electron trajectories are marked by arrows. The starting points of the trajectories indicate the tunneling exits and the endpoints of the trajectories represent electrons' positions at the moment of recollision.

The angular momentum of the driving light field is closely related to the dynamics of intense-light-matter interaction [37]. As known, light field's ellipticity is directly associated with its spin angular momentum (SAM) [38]. Due to the angular momentum conservation, the SAM of the radiated harmonic field is essentially transferred from the orbital angular momentum (OAM) of recollision electrons at the moment of recombination. In the classical picture, the OAM ($\mathbf{L}$) can be expressed as the cross product of electron's velocity ($\mathbf{v}$) and the distance to the nucleus ($\mathbf{r}$) [see Fig. 3(a)], i.e., $\mathbf{L} = \mathbf{r} \times \mathbf{v}$. Therefore, the harmonic helicity is closely related to the electron trajectories.

As shown in Fig. 3, for each crossing angle, trajectory A recollides with the nucleus with a positive OAM ($\mathbf{L}$ is inwards perpendicular to the x-y plane). One can notice that the

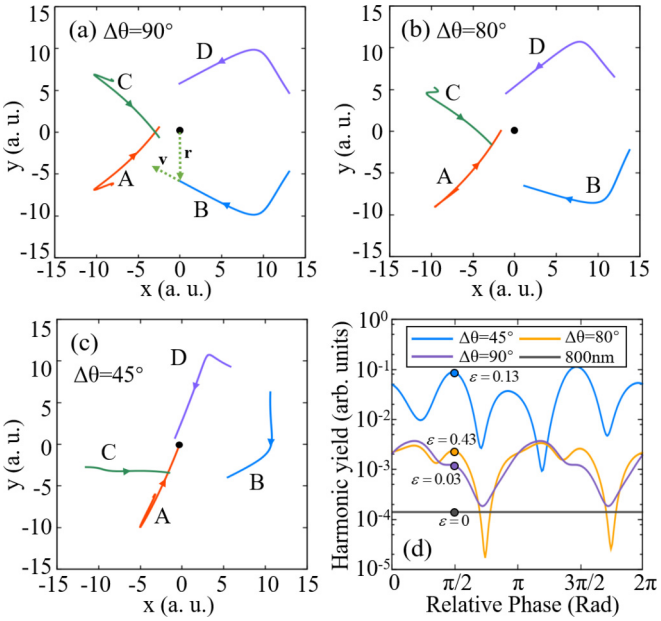

FIG. 3. (a)–(c) The quantum orbits in the different cross-linearly-polarized laser fields whose crossing angles are (a) $\Delta\theta = 90^\circ$, (b) $\Delta\theta = 80^\circ$, and (c) $\Delta\theta = 45^\circ$, respectively. (d) Comparison of the 28th harmonic yields between different laser fields. For comparison, the intensity of the single-color 800-nm linearly polarized light field (black line) is chosen to be 1.4×10^{14} W/cm^2, which is the same as the intensity of the two-color light fields (blue, yellow, and purple lines). In (d), some typical ellipticity values of harmonics are marked.

ellipticity of the corresponding harmonic burst is also positive, as shown in Fig. 2. As for trajectory C, it recombines with the nucleus with a negative OAM ($\mathbf{L}$ is outwards perpendicular to the x-y plane). Its corresponding harmonic burst also has a negative ellipticity. Besides, trajectories A and C are symmetric at $\Delta\theta = 90^\circ$ [Fig. 3(a)]. In this case, the OAMs values of these two recollision electron wave packets are exactly opposite as well as their induced harmonic ellipticity [see Fig. 2(a2)]. When the crossing angle becomes $\Delta\theta = 80^\circ$ [Fig. 3(b)], the symmetry between the electron trajectories is slightly broken. Compared with the case of $\Delta\theta = 90^\circ$, the velocities and positions of the recollision electrons are shifted. Trajectory A is dragged towards the nucleus and meanwhile, trajectory C is dragged away from the nucleus. Consequently, their induced harmonic radiations have asymmetrical ellipticities [see Fig. 2(b2)]. If the crossing angle is further reduced to $\Delta\theta = 45^\circ$, the electron trajectory A collides with the nucleus straightly ($\mathbf{L} \sim 0$). That is why the generated harmonic has a very small ellipticity [see Fig. 2(c2)].

One may notice that the exit points of trajectories B and D are counterintuitive, which is not opposite to the direction of the instantaneous electric field. Here, we have to stress that the trajectory calculated within saddle point approximation is a special trajectory in an electron wave packet. This special trajectory has the maximum recollision probability for the electron. However, the electron wave packets B and D actually tend to be directly ionized. Therefore, in order to satisfy the return condition [Eq. (6)], the initial states of the electron trajectory for B and D are rigorous, leading to the

counterintuitive exit points. Besides, it should be noted that the though the electric field A (C) and B (d) are symmetrical in the Lissajous diagram (Fig. 2), the temporal evolutions of the electric fields are different for the corresponding trajectories [39]. Thus, these electron trajectories are asymmetrical.

C. Analysis of the SAM of the driving light field

As shown in Fig. 1, the relative phase and the crossing angle have different effects on modulating the harmonic ellipticity. To inspect the origin of such difference between these two parameters, we now focus on the SAM of the driving laser fields. Recently, the dual symmetric Lagrangian formulation of classical electromagnetism was put forward by Bliokh and coworkers [40,41]. Compared with the standard field-theory formulation of electromagnetism, the dual electromagnetism ensures a self-consistent separation of the spin and orbital degrees of freedom [40]. Here, we adopt this dual-symmetry formalism to calculate the SAM density, $\mathbf{S}$, of the two-color light field:

$$\mathbf{S} = \tfrac{1}{2}(\mathbf{E}\times\mathbf{A} + \mathbf{B}\times\mathbf{C}), \tag{10}$$

in which $\mathbf{E}$ is the electric field, $\mathbf{A}$ is the electric vector potential, $\mathbf{B}$ is the magnetic field, and $\mathbf{C}$ is the magnetic vector potential. In the Coulomb gauge $\nabla\cdot\mathbf{A}=0$, the electric and magnetic fields can be expressed via the vector potential as $\mathbf{E}=-\partial_t\mathbf{A}$, $\mathbf{B}=\nabla\times\mathbf{A}$, $\mathbf{B}=-\partial_t\mathbf{C}$ and $\mathbf{E}=-\nabla\times\mathbf{C}$. With the approximation $f'(t)=0$, the electric vector potential can be expressed as

$$\begin{aligned}\mathbf{A}(t) = \Bigg[&-\frac{E_{800}f(t)}{\omega_{800}}\sin(\omega_{800}t)\\ &-\frac{E_{400}f(t)}{\omega_{400}}\cos(\Delta\theta)\sin(\omega_{400}t-\Delta\varphi)\Bigg]\mathbf{e}_y\\ &-\frac{E_{400}f(t)}{\omega_{400}}\sin(\Delta\theta)\sin(\omega_{400}t-\Delta\varphi)\mathbf{e}_x,\end{aligned} \tag{11}$$

Since HHG process is dominated by the electric field of light [4], we neglect the magnetic field portion in Eq. (10). And then, we substitute the electric field [Eq. (4)] and the electric vector potential [Eq. (11)] into the expression of SAM density [Eq. (10)]. After the simplification, we will finally have

$$\begin{aligned}\mathbf{S} = &\frac{1}{2}E_{800}E_{400}[f(t)]^2\sin(\Delta\theta)\mathbf{e}_z\\ &\times\Bigg[\frac{1}{\omega_{400}}\cos(\omega_{800}t)\sin(\omega_{400}t-\Delta\varphi)\\ &-\frac{1}{\omega_{800}}\sin(\omega_{800}t)\cos(\omega_{400}t-\Delta\varphi)\Bigg].\end{aligned} \tag{12}$$

In our configuration, the longitudinal component of electric fields is ignored, and hence only the z-component SAM density exists.

According to Eq. (12), the SAM density of the two-color field is a function of time, crossing angle, and relative phase. And, it can be noticed that the crossing angle affects the magnitude of light's SAM density, but it imposes little effect on the sign of SAM density. As for the relative phase, it can significantly affect both. The influence of the crossing angle and the relative phase on the instantaneous SAM density of the driving field coincides with that on the harmonic ellipticity. There is an intrinsic correlation between the SAM of driving laser fields and the high-order-harmonic ellipticity in the HHG process.

As known, for a single-color elliptical light field, the SAM is dependent on the relative phase between its two orthogonal field components. As for two-color cross-linearly-polarized light fields, the SAM is also associated with the relative phase between the 800- and 400-nm components. Here, the largest difference between these two fields is that the SAM of the two-color fields is time-dependent, as indicated by Eq. (12). Such a unique feature leads to an important consequence that the photoelectrons ionized at different instants will obtain different angular momentums from the driving light field. For each crossing angle, electrons ionized at the driving field peaks A and B "feel" an anticlockwise electric field during their classical motion [see Fig. 2(a1)]. Also, the electrons will possess positive OAMs in recollision. As for the electrons ionized at the peaks C and D, they "feel" a clockwise electric field after tunneling, and hence their OAMs turn to be negative. These different OAMs transfer to the emitted high-energy photons at different recollision times, therefore manifesting the time-dependent ellipticity for the harmonic bursts, as shown in Fig. 2. Furthermore, when the relative phase of the two-color field is increased by π, the shape of the field's Lissajous curve will remain the same. Therefore, the ellipticities of harmonics are periodically controlled by the relative phase with the cycle of π, as shown in Figs. 1(c)–1(f).

In Fig. 3(d), we further compare the 28th harmonic yields in two-color cross-linearly-polarized laser fields with that in a single-color 800-nm linearly polarized light field. Here, the intensity of the 800-nm field (I'_{800}) is chosen to be $1.4\times10^{14}\mathrm{W/cm^2}$, which is the same as the intensity of the two-color fields used previously, i.e., $I'_{800}=I_{800}+I_{400}$. Interestingly, one can find that, at most relative phases, the harmonic yields driven by the two-color laser fields can be larger than that driven by the single 800-nm light field [Fig. 3(d)]. When driving by a single-color laser field, the harmonic yields are typically extremely low when the polarization is not close to linear. However, it is different in the case of two-color driving laser field. The enhancement of harmonic yields in a two-color laser field has been widely studied [20,35,42,43]. In brief, the traveling time of electrons in a two-color laser field is much smaller than that in an 800-nm linearly polarized field, so the electron wave-packet spreading effect is significantly weaken. Moreover, when the crossing angle is large, the electron wave packet at the time of ionization is denser. Therefore, the harmonic yield in the two-color laser field can be several orders of magnitude higher than that by using the 800-nm linearly polarized field.

IV. GENERATING HELICAL ATTOSECOND PULSE IN TWO-COLOR CROSS-LINEARLY-POLARIZED LASER FIELD

As known, HHG is an important method to produce attosecond pulses [2,44]. A natural interest is whether one can employ two-color cross-linearly-polarized laser fields to further control the helicity of the attosecond pulse produced in

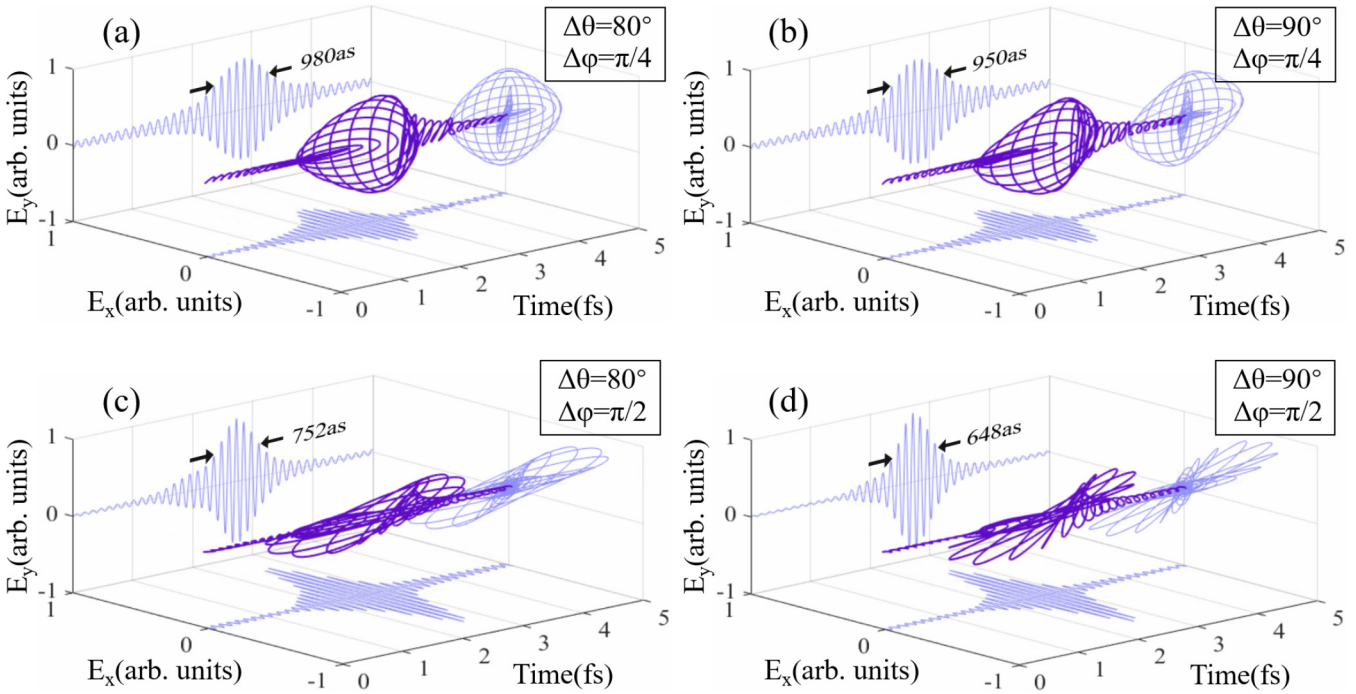

FIG. 4. Attosecond wave forms of the produced isolated attosecond pulses in the high-order harmonic generation driven by few-cycle ($\tau_{800,\mathrm{FWHM}} = \tau_{400,\mathrm{FWHM}} = 2$ fs) two-color cross-linearly-polarized laser fields. The corresponding carrier-envelop-phase of the 400-nm light field and the crossing angle are presented in the inset.

HHG [45]. Here, we consider a few-cycle two-color cross-linearly-polarized driving laser fields whose mathematical description is also given by Eq. (4) and the pulse duration of the 800-nm and 400-nm components are $\tau = 2$fs (FWHM). In Fig. 4, we present the wave forms of the attosecond pulses calculated by Fourier transformation of the corresponding harmonic spectra, in which the harmonics above the 20th are preserved to obtain the synthesized pulses. Using the few-cycle pulses for the driving laser fields, the produced radiation is confined to an isolated pulse of attosecond emission [46]. The pulse durations (at the amplitude FWHM) of the generated isolated pulses are nearly 950 as [Figs. 4(a) and 4(b)] and 700 as [Fig. 4(c) and 4(d)], respectively.

The projection of the isolated attosecond pulses over the plane of the electric field shows the helicity of the pulses. In general, through adjusting the crossing angle and the relative phase, the ellipticity can be tuned. At $\Delta\theta = 80^\circ$ and $\Delta\varphi = \pi/4$, the attosecond pulse can reach a high ellipticity ($|\varepsilon| \sim 0.5$ at the peak field) [Fig. 4(a)]. As for $\Delta\varphi = \pi/2$, the produced attosecond pulse is almost linearly polarized ($|\varepsilon| \sim 0.1$ at the peak field) [Fig. 4(c)]. Also, if enlarging the crossing angle [Fig. 4(b) and 4(d)], the ellipticity of the attosecond pulses will accordingly decrease. Such ellipticity controllability is attributed to the change of the amplitude ratio and the phase delay between the x and y component of the synthesized attosecond pulses. The simulations indicate that it would be an effective method to generate an elliptical attosecond pulse and control its ellipticity with few-cycle two-color cross-linearly-polarized driving fields.

V. CONCLUSION

In summary, we have investigated the capability of two-color cross-linearly-polarized laser fields in controlling the ellipticity of high-order harmonics. Through finely adjusting the crossing angle and the relative phase of the driving laser fields, harmonic ellipticity can be fully controlled. We reveal that the harmonic helicity depends on the unsymmetrical contribution between the quantum orbits. When adjusting the relative phase and the crossing angle, the temporal structure of light's SAM is manipulated, which accordingly affects the angular momentum transfer process in HHG. In the same light field configuration, we have also illustrated the probability of producing chiral isolated attosecond pulses. This work shows the inherent relationship between the driving field's time-dependent SAM structure and the produced harmonic features, which has been rarely recognized. Meanwhile, the calculation results will facilitate the employment of the two-color laser fields in producing helical high-order harmonics and attosecond pulses.

ACKNOWLEDGMENTS

This work was supported by the NSFC (Grants No. 92050201 and No. 11774013).

[1] F. Krausz and M. Yu. Ivanov, Rev. Mod. Phys. **81**, 163 (2009).

[2] T. Gaumnitz, A. Jain, Y. Pertot, M. Huppert, I. Jordan, F. A. Lamas, and H. J. Wörner, Opt. Express **25**, 27506 (2017).

[3] M. Hentschel *et al.*, Nature (London) **414**, 509 (2001).
[4] P. B. Corkum, Phys. Rev. Lett. **71**, 1994 (1993).
[5] A. Ferré *et al.*, Nat. Photonics **9**, 93 (2015).
[6] V. V. Strelkov, A. A. Gonoskov, I. A. Gonoskov, and M. Yu. Ryabikin, Phys. Rev. Lett. **107**, 043902 (2011).
[7] K. S. Budil, P. Salieres, A. L'Huillier, T. Ditmire, and M. D. Perry, Phys. Rev. A **48**, R3437 (1993).
[8] P. Antoine, B. Carré, A. L'Huillier, and M. Lewenstein, Phys. Rev. A **55**, 1314 (1997).
[9] J. Levesque, Y. Mairesse, N. Dudovich, H. Pepin, J.-C. Kieffer, P. B. Corkum, and D. M. Villeneuve, Phys. Rev. Lett. **99**, 243001 (2007).
[10] X. Zhou, R. Lock, N. Wagner, W. Li, H. C. Kapteyn, and M. M. Murnane, Phys. Rev. Lett. **102**, 073902 (2009).
[11] B. Vodungbo *et al.*, Opt. Express **19**, 4346 (2011).
[12] A. Fleischer, P. Sidorenko, and O. Cohen, Opt. Lett. **38**, 223 (2013).
[13] A. Fleischer, O. Kfir, T. Diskin, P. Sidorenko, and O. Cohen, Nat. Photonics **8**, 543 (2014).
[14] O. Kfir *et al.*, Nat. Photonics **9**, 99 (2015).
[15] D. D. Hickstein *et al.*, Nat. Photonics **9**, 743 (2015).
[16] C. Hernández-García, C. G. Durfee, D. D. Hickstein, T. Popmintchev, A. Meier, M. M. Murnane, H. C. Kapteyn, I. J. Sola, A. Jaron-Becker, and A. Becker, Phys. Rev. A **93**, 043855 (2016).
[17] P.-C. Huang, C. Hernández-García, J.-T. Huang, P.-Y. Huang, C.-H. Lu, L. Rego, D. D. Hickstein, J. L. Ellis, A. Jaron-Becker, and A. Becker, Nat. Photonics **12**, 349 (2018).
[18] D. Azoury, O. Kneller, M. Krüger, B. D. Bruner, O. Cohen, Y. Mairesse, and N. Dudovich, Nat. Photonics **13**, 198 (2019).
[19] D. Peng, L.-W. Pi, M. V. Frolov, and A. F. Starace, Phys. Rev. A **95**, 033413 (2017).
[20] I. J. Kim, C. M. Kim, H. T. Kim, G. H. Lee, Y. S. Lee, J. Y. Park, D. J. Cho, and C. H. Nam, Phys. Rev. Lett. **94**, 243901 (2005).
[21] D. Shafir *et al.*, Nature (London) **485**, 343 (2012).
[22] J. Zhao and M. Lein, Phys. Rev. Lett. **111**, 043901 (2013).
[23] Y. Chou, P.-C. Li, T.-S. Ho, and Shih-I. Chu, Phys. Rev. A **91**, 063408 (2015).
[24] E. J. Takahashi, P. F. Lan, O. D. Mücke, Y. Nabekawa, and K. Midorikawa, Phys. Rev. Lett. **104**, 233901 (2010).
[25] G. Lambert *et al.*, Nat. Commun. **6**, 6167 (2015).
[26] B. Mahieu, S. Stremoukhov, D. Gauthier, C. Spezzani, C. Alves, B. Vodungbo, P. Zeitoun, V. Malka, G. De Ninno, and G. Lambert, Phys. Rev. A **97**, 043857 (2018).
[27] C. Zhai, R. Shao, P. Lan, B. Wang, Y. Zhang, H. Yuan, S. M. Njoroge, L. He, and P. Lu, Phys. Rev. A **101**, 053407 (2020).
[28] S. Stremoukhov, A. Andreev, B. Vodungbo, P. Salières, B. Mahieu, and G. Lambert, Phys. Rev. A **94**, 013855 (2016).
[29] A.-T. Le, H. Wei, C. Jin, and C. D. Lin, J. Phys. B **49**, 053001 (2016).
[30] A. D. Bandrauk, S. Chelkowski, S. Kawai, and H. Z. Lu, Phys. Rev. Lett. **101**, 153901 (2008).
[31] R. Kopold, W. Becker, and M. Kleber, Opt. Commun. **179**, 39 (2000).
[32] L. Medišauskas, J. Wragg, H. van der Hart, and M. Y. Ivanov, Phys. Rev. Lett. **115**, 153001 (2015).
[33] J. A. Pérez-Hernández, L. Roso, and L. Plaja, Opt. Express **17**, 9891 (2009).
[34] L. Zhang, X. Xie, S. Roither, D. Kartashov, Y. Wang, C. Wang, M. Schöffler, D. Shafir, P. B. Corkum, A. Baltuška *et al.*, Phys. Rev. A **90**, 061401(R) (2014).
[35] C. M. Kim and C. H. Nam, J. Phys. B **39**, 3199 (2006).
[36] Y. Li, X. Zhu, Q. Zhang, M. Qin, and P. Lu, Opt. Express **21**, 4896 (2013).
[37] Y. Fang, M. Han, P. Ge, Z. Guo, X. Yu, Y. Deng, C. Wu, Q. Gong, and Y. Liu, Nat. Photonics **15**, 115 (2021).
[38] R. Beth, Phys. Rev. **50**, 115 (1936).
[39] Y. Fang, C. He, M. Han, P. Ge, X. Yu, X. Ma, Y. Deng, and Y. Liu, Phys. Rev. A **100**, 013414 (2019).
[40] K. Y. Bliokh, A. Y. Bekshaev, and F. Nori, New J. Phys. **15**, 033026 (2013).
[41] K. Y. Bliokh, J. Dressel, and F. Nori, New J. Phys. **16**, 093037 (2014).
[42] L. Brugnera *et al.*, Opt. Lett. **35**, 3994 (2010).
[43] E. Cormier and M. Lewenstein, Eur. Phys. J. D **12**, 227 (2000).
[44] K. M. Dorney *et al.*, Phys. Rev. Lett. **119**, 063201 (2017).
[45] C. Ruiz, D. J. Hoffmann, R. Torres, L. E. Chipperfield, and J. P. Marangos, New. J. Phys. **11**, 113045 (2009).
[46] E. Goulielmakis *et al.*, Science **320**, 1614 (2008).